buildings

MDPI

Article

Influence of Support Equivalent Stiffness on Stability Capacity of Concrete-Pier-Supported Elliptical Cylindrical Double-Layer Reticulated Shell

Pengfei Ma [1,2,*] and Shuming Jia [1,2]

1 College of Civil Engineering, Lanzhou Institute of Technology, Lanzhou 730050, China
2 Gansu Technology Center of Green and Intelligent Construction, Lanzhou 730050, China
* Correspondence: vip_lom@163.com

Abstract

Concrete pier-supported double-layer reticulated shells are widely used in long-span industrial buildings, yet the influence of support equivalent stiffness on structural stability remains insufficiently understood. This study investigates the stability behavior of an elliptical cylindrical double-layer reticulated shell supported by concrete piers with steel bearings. A simplified calculation method for equivalent support stiffness is derived based on a series cantilever system model and validated numerically. Seven steel bearing web thicknesses (10–40 mm) commonly used in engineering practice are selected, yielding equivalent stiffness coefficients ranging from 0.017 to 0.065. Eigenvalue buckling analysis is performed, and three quantitative indicators—critical load factor, sensitivity, and saturation degree—are introduced to systematically evaluate the effect of equivalent stiffness on stability capacity. Results show that the equivalent stiffness coefficient is typically less than 0.1, and using rigid links (infinite stiffness) overestimates the stability capacity by approximately 7% compared with the lowest stiffness case. The sensitivity of stability capacity to stiffness decreases monotonically as equivalent stiffness increases, with a threshold identified at $\xi = 0.05$. When the saturation degree of the critical load factor exceeds 72%, further increasing equivalent stiffness yields diminishing returns. Buckling modes transition from local end uplift to overall lateral tilting as equivalent stiffness increases. These findings provide a theoretical basis for selecting rational support stiffness values in the design of concrete-pier-supported reticulated shell structures.

Keywords: double-layer reticulated shell; equivalent stiffness; stability capacity; eigenvalue buckling; sensitivity analysis; concrete pier support

Check for updates

Academic Editor: Vipul Patel

Received: 18 August 2026
Revised: 13 September 2026
Accepted: 18 September 2026
Published: 20 September 2026

1. Introduction

Spatial grid structures have been widely adopted in long-span public and industrial buildings due to their rational load-bearing behavior, light self-weight, high stiffness, and geometric flexibility [1]. These structural systems can cover large spans with relatively small member sections, making them particularly suitable for sports stadiums, airport terminals, convention centers, and industrial facilities such as storage sheds and coal bunkers. Chilton noted that through the optimization of geometric topology, spatial grid structures maximize material utilization, thereby providing an efficient structural solution for long-span buildings [1]. In recent years, free-form spatial grid structures have become increasingly common in large public buildings, where the grid layout influences both mechanical performance and architectural aesthetics. Liu et al. found that the topological form of a free-form spatial grid often has a greater effect on its mechanical behavior than the member material or cross-sectional dimensions [2].

With the rapid economic development and urbanization in China, the demand for long-span space structures has grown considerably to accommodate various cultural, sports, transportation, and social activities. Significant progress has been made in the engineering practice of such structures. Xue Suduo showed that various types of spatial structural systems have been successfully applied in sports stadiums, convention centers, entertainment venues, airport terminals, factories, and warehouses, among which spatial grid structures have become a primary form for airport terminals and stadiums [3]. Benefiting from their superior spanning capability and architectural expression, spatial grid structures are among the most preferred options for long-span buildings. Chen et al. proposed an equivalent model simplification method for failure-state analysis of innovative spatial grid arch structures, which has been successfully applied to landmark public buildings such as museums, exhibition centers, and gymnasiums [4]. From planar grids and cylindrical reticulated shells to spatial dome-shaped grids and free-form grids, these diverse structural forms continue to expand the boundaries of spatial grid structural systems [5–8].

However, the large span and high flexibility of long-span spatial grid structures often make stability capacity a controlling factor in design and analysis. Unlike traditional low- and mid-rise buildings, long-span space structures must satisfy not only strength requirements but also global stability under external loads. Numerous engineering practices and studies have demonstrated that the instability of reticulated shells tends to occur suddenly without obvious warning, potentially leading to complete collapse. The collapse of a 93.5 m single-layer reticulated shell roof in Bucharest in 1963 under heavy snow, and the overturning of a coal bunker composite reticulated shell during construction in Changzhi, Shanxi Province in 1993, brought the issue of shell stability to the forefront [9]. Since then, the stability of long-span single-layer reticulated shells has been extensively and intensively studied worldwide. Ferretti et al. proposed an equivalent Timoshenko beam model incorporating prestressing effects for the buckling analysis of periodic micro-structured beams, providing theoretical support for understanding the buckling behavior of spatial grid structures [10]. Recent advances in shell mechanics have moved from deterministic analysis toward stochastic frameworks that account for material parameter variability. Xiang et al. [11] developed a perturbation stochastic meshless method without partial derivatives for the free vibration analysis of FG-CNTRC conical shell panels, incorporating the spatial randomness of material properties into a first-order shear deformation shell formulation. Their work demonstrates the efficiency of stochastic meshless frameworks for low-uncertainty shell problems, providing a methodological reference for uncertainty quantification in shell-type structures.

Gioncu systematically reviewed the history of reticulated shell stability research, summarized various instability modes, and investigated the propagation of local buckling [9]. Tian et al. studied the collapse-resistant performance of long-span single-layer spatial grid structures subjected to equivalent sudden joint loads, revealing the failure mechanisms of spatial structures under extreme loading [12]. Current research results and engineering experience indicate that the stability of reticulated shells has surpassed strength and stiffness issues to become the governing factor in their design. Luo et al. conducted an in-depth study on the buckling instability of in-service space grid steel tubes using an image-vision-based prediction method, pointing out that initial bending deformations of members may develop into significant buckling deformations as the load increases [13]. A dynamic experimental study on the progressive collapse resistance of a polyline-shaped long-span double-layer grid space structure revealed the collapse mechanisms under different failure locations, showing that the top chord is a key component in collapse-resistant design [7]. Zhou et al. investigated the distribution of survival space in grid structures under overload collapse, demonstrating how different loading regions affect collapse behavior and survival space patterns [6]. For any new structural system, the static load-bearing capacity (including failure state, failure mode, and ultimate load) is an essential research topic to ensure safe operation.

The current technical specification for space frame structures (JGJ 7-2010) explicitly states that when performing independent verification of an upper space grid structure, the influence of the lower supporting structure should be considered by converting it into equivalent stiffness and equivalent mass as boundary conditions for the upper structure analysis [14]. The specification also notes that reasonable boundary constraints should be determined based on the actual construction details of the support joints and the stiffness of the supporting structure. This provision highlights the engineering significance of properly determining the equivalent stiffness at supports for stability analysis of spatial grid structures. For large space truss structures, Liu et al. proposed an equivalent continuum modeling method considering nonlinear elastic joints, deriving an equivalent 8-degree-of-freedom nonlinear beam element based on the energy equivalence method, and verified the correctness and efficiency of the method through numerical examples [15]. Wang Yuan et al. showed that replacing concrete supports with fixed, hinged, or sliding supports fails to accurately reflect the actual stress state of the structure; concrete supports significantly affect the overall performance of large-span space grid structure models, and the results of integrated structural models tend to be more unfavorable [16]. Therefore, it is necessary to consider the cooperative work between the space structure and the lower concrete supports.

In the field of industrial buildings, concrete pier-type reticulated shell structures are very common—the lower part consists of concrete piers with relatively large cross-sections, and the upper space grid structure is connected via steel supports. Gao Yan et al., using the flat grid roof of a coal industry plant as a background, solved for the equivalent spring stiffness of cantilever column supports based on mechanics of materials theory, clarifying the calculation methods for tangential, normal, and elastic support constraints [17]. In such systems, the concrete pier and the steel support form a series cantilever system, and the overall equivalent stiffness directly affects the boundary constraint conditions of the upper reticulated shell, thereby influencing the structural stability capacity. Hence, a thorough understanding of the influence of equivalent stiffness on the stability capacity of this type of building is key to ensuring design safety and economy. Currently, there is relatively little research on the cooperative work between the upper space structure and the lower supporting structure, especially regarding the sensitivity and saturation characteristics of the contribution of equivalent stiffness to stability capacity. The design of elastic grid structures, as a lightweight, material-efficient structural form, requires a balance between material resources and architectural, structural, and environmental factors [18].

Equivalent support stiffness is a well-established concept in the analysis of space frame structures. However, for concrete-pier-supported elliptical cylindrical double-layer reticulated shells, previous studies have not systematically quantified how the equivalent stiffness of the pier–steel bearing series system affects the stability capacity. Therefore, the novelty of this study is not the concept of equivalent stiffness itself, but the following two aspects. First, for large-section concrete pier supports, a simplified estimation method for the equivalent stiffness is derived from a series cantilever model. This method is intended to provide an order-of-magnitude parameter range for scientific studies when a refined pier–bearing model is not available; it is not intended to determine an exact equivalent stiffness. Second, two quantitative indicators—sensitivity S and saturation degree D—are introduced to characterize the influence of equivalent stiffness on stability capacity. The sensitivity describes the marginal gain in the critical load factor as the equivalent stiffness increases, while the saturation degree measures how close the current support condition is to the rigid-link upper bound. These indicators make it possible to identify the transition from a sensitive range to an insensitive range and to evaluate the diminishing returns of increasing stiffness. Based on these two aspects, seven equivalent stiffness coefficients (ξ = 0.017–0.065) corresponding to steel bearing web thicknesses of 10–40 mm are selected, and eigenvalue buckling analysis is performed to examine the critical load factor, sensitivity, saturation, and buckling mode evolution. The results provide a theoretical basis for selecting rational support stiffness values for concrete-pier-supported reticulated shell structures.

2. Numerical Model

To thoroughly investigate the influence of bearing equivalent stiffness on the stability capacity of the upper spatial latticed shell structure, this study establishes a three-dimensional model of the upper spatial latticed shell based on a general design scheme of an actual storage shed project (Figure 1a), with a top view shown in Figure 1b. The model is developed using the general-purpose structural analysis software SAP2000 27.x. The overall shape is an elliptical cylinder, with a plan span of 85 m, length of 160 m, rise height of 34 m, and a rise-to-span ratio of approximately 1/2.5 (Figure 1c). The spatial latticed shell adopts a quadrangular pyramid as the basic unit, with a pyramid height of 2.5 m and a base side length of approximately 4 m; detailed dimensions are shown in Figure 1d.

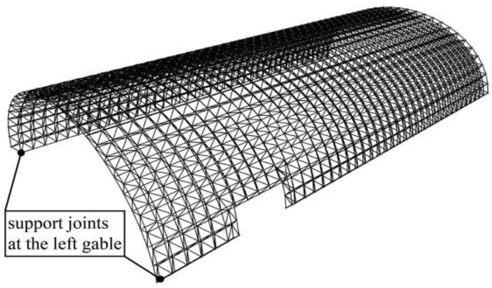

(**a**) latticed shell model

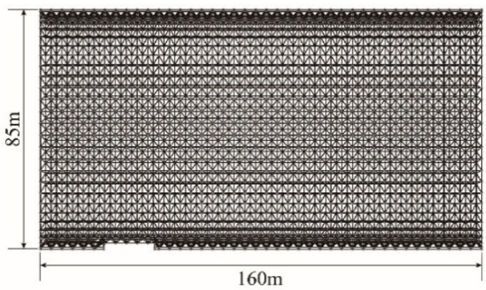

(**b**) top view

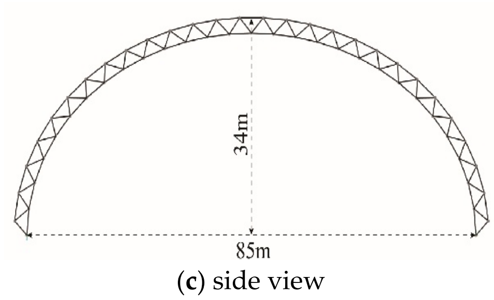

(**c**) side view

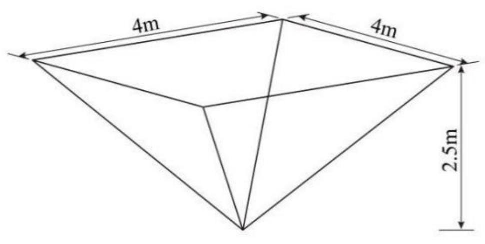

(**d**) quadrangular pyramid

Figure 1. Numerical calculation model.

For double-layer spatial latticed shell structures, bolted spherical joints are commonly used in engineering practice, and they are typically simplified as hinged connections in analytical models [14]; each member is assumed to be a truss element. Since SAP2000's element library does not contain a dedicated truss element, this study uses frame elements (beam elements) combined with end-release techniques (releasing major bending moment, minor bending moment, and torque at beam ends) to simulate the mechanical behavior of truss elements. All members in the model are circular steel tubes, with a maximum cross-section of $\Phi180 \times 12$ and a minimum of $\Phi75.5 \times 3.75$. The material is Q235B steel, and the material parameters adopt the standard values specified in the Chinese code embedded in the software.

The support joints of the model use single-point link elements to simulate lateral stiffness. The local 1-axis of the element is along the width direction of the reticulated shell, and the equivalent stiffness is adopted to simulate different support constraints. The rotational and vertical degrees of freedom of the joints are both constrained, and the longitudinal degree of freedom is released to simulate support sliding that considers temperature effects in practical engineering. However, for the support joints at the left gable, the longitudinal translational degree of freedom is constrained to prevent overall longitudinal rigid-body displacement of the structure.

3. Loads and Analysis Method

Stability verification is a necessary step in the design of long-span spatial latticed shell structures. In engineering design, eigenvalue buckling analysis is commonly used to verify the stability of latticed shell systems. This method accounts for geometric stiffness and aims to determine the theoretical critical buckling load and the corresponding buckling mode. The governing equation is the generalized eigenvalue problem shown in Equation (1):

$$(\boldsymbol{K} - \lambda \boldsymbol{K}_G)\boldsymbol{\phi} = 0 \tag{1}$$

where: $\boldsymbol{K}$ is the elastic stiffness matrix, $\boldsymbol{K}_G$ is the geometric stiffness matrix, λ is the buckling load factor, and the critical buckling load factor is denoted as λ_{cr}, and the corresponding critical buckling load is $\boldsymbol{P}_{\mathrm{cr}} = \lambda_{\mathrm{cr}}\boldsymbol{P}_{\mathrm{ref}}$, with $\boldsymbol{P}_{\mathrm{ref}}$ being the reference load.

This study evaluates the stability of the double-layer elliptical cylindrical latticed shell using eigenvalue buckling analysis. Long-span spatial latticed shell buildings have large open spaces, and external loads (e.g., wind load, snow load) are often non-uniformly distributed; in particular, the edge regions of the structure typically experience higher loads [19]. Therefore, a surface-normal pressure load is applied to the edge regions of the latticed shell. In eigenvalue buckling analysis, the magnitude of the reference load does not affect the computed results; in this study, a uniform value of 1 kN/m^2 is adopted. The specific load application region is shown in Figure 2.

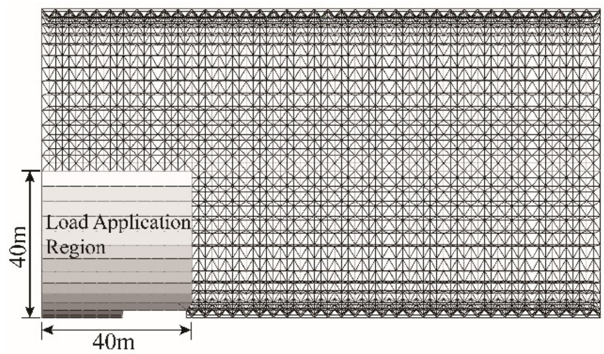

Figure 2. Load application region.

4. Setting of Equivalent Stiffness Levels

When performing an independent stability analysis of a spatial latticed shell system, it is necessary to consider the equivalent stiffness at the supports. This paper focuses on the commonly encountered concrete pier-supported spatial latticed shell structures in industrial buildings. In such systems, the substructure consists of concrete piers, which typically have large cross-sectional dimensions, with the strong-axis dimension larger than the weak-axis dimension. The strong axis is generally oriented to resist lateral forces transmitted from the upper latticed shell. Steel bearings are installed at the top of the concrete piers to connect the upper latticed shell. The bearing height is generally 300–500 mm, and the bearings are free to slide longitudinally to accommodate thermal deformations (Figure 3). In order to ensure that the equivalent stiffness levels in this paper are comparable in order of magnitude to those in actual engineering, the equivalent stiffness of this type of large-section concrete pier support structure is first reasonably estimated. Based on the characteristics of this type of lower supporting structure, the following assumptions are proposed:

(i) The concrete pier and the steel bearing form a series cantilever system;
(ii) The concrete pier effectively restrains the bottom of the steel bearing, preventing rotational deformation;
(iii) For the steel bearing, only the transverse web provides the lateral stiffness.

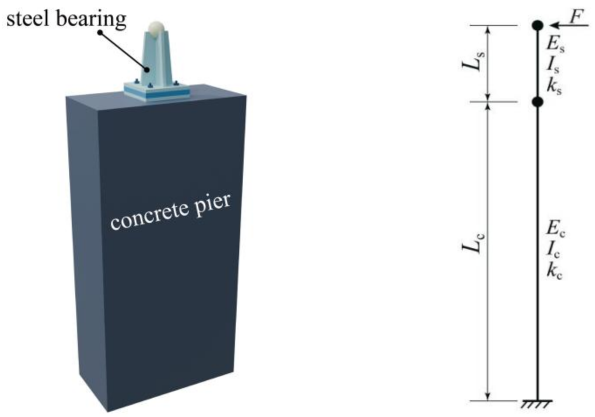

(**a**) three-dimensional view (**b**) mechanical model

Figure 3. Series cantilever system.

The equivalent stiffness is defined as the reaction force required to produce a unit displacement at the free end of the pier-steel bearing cantilever system. The mechanical model is shown in Figure 3. Let k_s and Δ_s denote the lateral stiffness and lateral displacement of the steel bearing, respectively, and k_c and Δ_c denote the lateral stiffness and lateral displacement of the concrete pier, respectively. Neglecting the contribution of the pier's end moment to the lateral displacement, the series system satisfies Equation (2):

$$\begin{cases} k_s\Delta_s = k_c\Delta_c = F \\ \Delta = \Delta_s + \Delta_c \end{cases} \tag{2}$$

where: Δ is the total lateral displacement. The lateral stiffness can be simplified using Equation (3):

$$\begin{cases} k_s = \frac{3E_sI_s}{L_s^3} \\ k_c = \frac{3E_cI_c}{L_c^3} \end{cases} \tag{3}$$

where: E_s, I_s, and L_s are the elastic modulus, moment of inertia, and length of the steel bearing, respectively; E_c, I_c, and L_c are the elastic modulus, moment of inertia, and length of the concrete pier, respectively. Combining Equations (2) and (3) yields the displacement ratio:

$$\frac{\Delta_s}{\Delta_c} = \frac{I_c}{I_s}\frac{E_c}{E_s}\left(\frac{L_s}{L_c}\right)^3 \tag{4}$$

Let $I_c/I_s = \alpha$. The elastic modulus of Q355B steel is approximately seven times that of C30 concrete. Based on practical engineering, the height ratio of the concrete pier to the steel bearing is $L_c/L_s \approx 4$. Substituting these into Equation (4) gives:

$$\frac{\Delta_s}{\Delta_c} = \frac{\alpha}{448} \tag{5}$$

The equivalent stiffness k satisfies:

$$\frac{1}{k} = \frac{1}{k_s} + \frac{1}{k_c} \tag{6}$$

Combining Equations (2), (5) and (6), the equivalent stiffness expressed in terms of the lateral stiffness of the concrete pier is obtained:

$$k = \frac{448}{\alpha + 448} k_c \tag{7}$$

To verify the practicality of this assumption, take a concrete cross-section of 500 mm × 1200 mm and a length L_c = 2 m, then the stiffness k_c = 810 kN/mm. For the steel bearing web of 150 mm × 20 mm, substituting into Equation (7) yields k = 28 kN/mm.

A numerical model was established as shown in Figure 4. The bottom of the model is a fixed end. A unit horizontal displacement is applied at the top, and the out-of-plane translational degree of freedom is constrained to ensure that deformation occurs in the plane. The vertical degree of freedom and rotational degrees of freedom remain free. There is no load within the spans of the pier and steel bearing in this model; only joint displacements occur. Its deflection curve is a cubic function, and the SAP2000 frame element adopts cubic displacement interpolation, so one element is divided for each part.

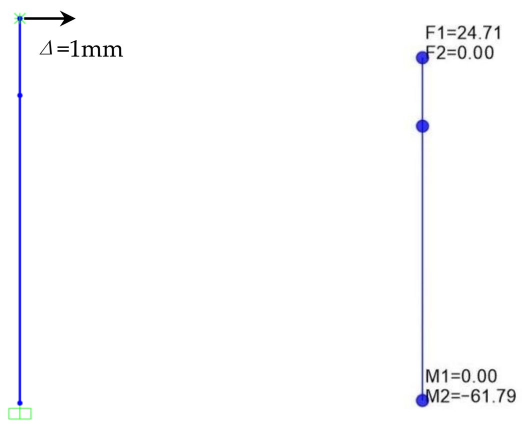

(**a**) series cantilever model (**b**) series cantilever model

Figure 4. Numerical model of the series cantilever system (Δ = 1 mm).

The numerical calculation result shows k = 24.7 kN/mm. It can be observed that the two results are close. The error mainly comes from two aspects. First, this paper assumes that the large-section concrete pier can effectively restrain the steel bearing from rotational displacement. However, when the steel bearing joint is subjected to a relatively large horizontal force, the top of the concrete pier is simultaneously subjected to a horizontal force and a moment; in addition to lateral displacement, there is also slight rotation. Second, the frame element in SAP2000 is based on Timoshenko beam theory and considers shear deformation, whereas the lateral stiffness in this paper is established based on Euler beam theory in traditional structural mechanics and does not consider shear deformation,

https://doi.org/10.3390/buildings16183737

resulting in a smaller lateral displacement value while the actual value is larger, which makes the calculated equivalent stiffness larger than the numerical result.

It is worth noting that the proposed formula is not intended to establish an accurate theoretical model of equivalent stiffness, and it cannot be used to directly calculate the exact value of equivalent stiffness. If it is necessary to reasonably estimate the equivalent stiffness of large-section concrete pier supports so as to provide parameter values of comparable order of magnitude for scientific research, this formula can provide a certain reference value.

Define the equivalent stiffness coefficient $\xi = 448/(\alpha + 448)$. Since $\alpha > 0$, $\xi < 1$; that is, the equivalent stiffness is always smaller than the lateral stiffness of the concrete pier. Directly using the pier's lateral stiffness would overestimate the overall stiffness. To investigate the influence of different equivalent stiffness values on the structural stability, according to the specifications of JGJ 7-2010 (Technical specification for space frame structures) [14,19], seven commonly used steel bearing web thicknesses (with a height of 150 mm) are selected. The concrete pier cross-section remains the same as before (500 mm × 1200 mm). The parameters are listed in Table 1. The equivalent stiffness coefficient ranges from 0.017 to 0.065, generally less than 0.1, meaning that the equivalent stiffness is less than one-tenth of the pier's lateral stiffness. For comparison, this study also considers a rigid link boundary condition, which corresponds to an equivalent stiffness approaching infinity.

Table 1. Equivalent stiffness values.

Web thickness (mm)	10	14	20	25	30	35	40
Equivalent stiffness coefficient (ξ)	0.017	0.024	0.034	0.042	0.050	0.058	0.065
Equivalent stiffness (k)	14	19	28	34	41	47	53

5. Analysis of Stability Results

5.1. Critical Load Factor

Using the link elements in SAP2000, the seven equivalent stiffness values obtained above are assigned to the axial stiffness of the link elements. For the reference case (rigid link, infinite stiffness), a hinge boundary condition is directly applied. Eigenvalue buckling analysis is performed, and the first-order buckling factor is extracted, which represents the critical load factor λ_{cr} of the structure. The calculated results for all cases are summarized in Table 2. Figure 5 shows the variation of λ_{cr} with ξ.

It can be observed that as the equivalent stiffness coefficient increases, the critical load factor also increases, but it always remains lower than the value under the rigid link constraint. This indicates that using a simple rigid link overestimates the stability capacity of the structure to some extent—approximately 7% higher than the case with ξ = 0.017. Meanwhile, the growth rate of the curve gradually slows down as the equivalent stiffness increases, suggesting that further increases in stiffness contribute less to the enhancement of stability capacity.

Table 2. Critical load factors.

Equivalent stiffness coefficient (ξ)	0.017	0.024	0.034	0.042	0.050	0.058	0.065	∞
Critical load factor (λ_{cr})	52.06	53.00	53.82	54.14	54.39	54.55	54.67	55.69

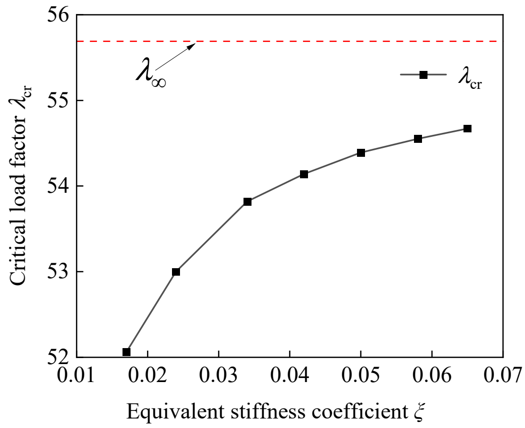

Figure 5. Relationship between critical load factor and equivalent stiffness coefficient.

5.2. Sensitivity Analysis

To quantitatively describe the feature that the critical load factor tends to level off as the equivalent stiffness coefficient increases, the sensitivity is defined as follows:

$$S = \frac{\left(\lambda_{cr}^{i+1} - \lambda_{cr}^{i}\right)/\lambda_{cr}^{i}}{(\xi_{i+1} - \xi_i)/\xi_i} \times 100\%, \qquad i = 1, 2, \ldots, 6 \tag{8}$$

where: λ_{cr}^{i} and λ_{cr}^{i+1} are two adjacent critical load factors, and ξ_i and ξ_{i+1} are the corresponding equivalent stiffness coefficients. Since only seven different equivalent stiffness coefficients are analyzed in this paper, the maximum value of i is taken as 6. The sensitivity S corresponding to each equivalent stiffness coefficient is calculated, and the S-ξ curve is plotted (as shown in Figure 6).

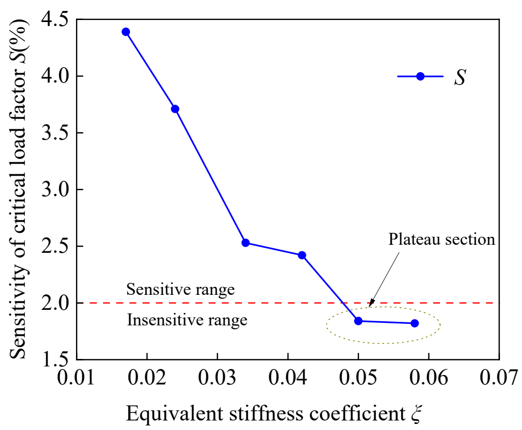

Figure 6. Sensitivity of critical load factor.

It can be seen that the sensitivity decreases continuously as ξ increases. In the sensitive range ($S \geq 2\%$), the curve decreases monotonically; after entering the insensitive range ($S < 2\%$), the sensitivity essentially stabilizes, and the rate of decrease diminishes significantly. For example, when $\xi = 0.058$, S = 1.82%, which is 58.5% lower than the highest value, indicating that further increases in stiffness no longer yield significant gains in stability capacity. The equivalent stiffness coefficient at this turning point is taken as the threshold for load-carrying capacity improvement. It can be seen that, for the example model in this paper, when the equivalent stiffness coefficient is 0.05, the critical load factor enters the insensitive range for the first time.

5.3. Saturation Analysis

As can be seen from Figure 5, simply setting the support condition of the latticed shell as a rigid link overestimates the critical buckling load to a certain extent. The rigid link corresponds to an equivalent stiffness approaching infinity, and the critical buckling load under this condition represents an upper bound of the structural stability capacity. It is worth noting that using eigenvalue buckling analysis to predict stability capacity is a rough approach. The actual stability capacity of the structure usually needs to consider factors such as geometric imperfections and geometric nonlinearity, and nonlinear buckling analysis techniques are required for prediction. To evaluate whether the current equivalent stiffness becomes the dominant factor controlling the load-carrying capacity, the saturation degree D is defined as follows:

$$D = \frac{\lambda_i - \lambda_{\min}}{\lambda_\infty - \lambda_{\min}} \times 100\% \tag{9}$$

where: λ_i is the critical load factor under each working condition, $\lambda_{\min}$ is the minimum among all critical load factors (in this paper, $\lambda_{\min}$ = 52.06), and λ_∞ is the critical load factor under the rigid link condition. The value of D ranges from 0% to 100%. A value closer to 100% indicates that the contribution of stiffness to the load-carrying capacity is nearly saturated and no longer governs the capacity; otherwise, there remains room for improvement.

Figure 7 shows the variation of D with ξ. As the equivalent stiffness coefficient increases, the cumulative contribution continuously increases and gradually approaches 100%. For this example model, it can be observed that when ξ = 0.065, D = 71.9%, indicating that there is still room for further improvement in stiffness. However, the sensitivity index clearly shows that as the equivalent stiffness continues to increase, there is a marginal effect on the stability capacity; that is, the capacity gain brought by a unit percentage increase in stiffness continues to decrease, meaning that the cost-effectiveness becomes increasingly lower. At this time, it is not recommended to continue considering using an increase in stiffness to exchange for an improvement in stability capacity.

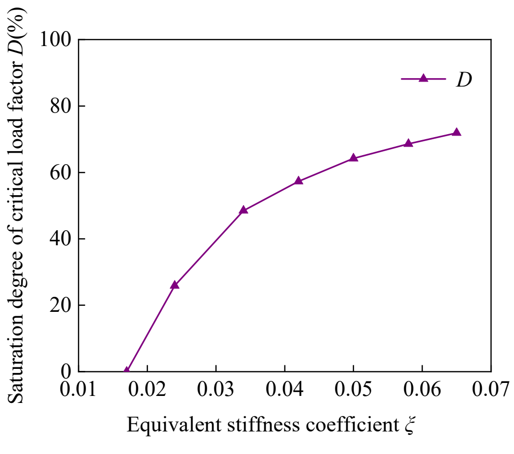

Figure 7. Saturation degree of critical load factor.

5.4. Buckling Modes

Figure 8 shows the buckling modes of the latticed shell under different equivalent stiffness coefficients. Based on the instability patterns, these modes can be classified into two major categories: (i) When the equivalent stiffness is relatively small (represented by ξ = 0.017), the instability manifests as a local uplift in the end region near the top, with insignificant deformation on both sides. (ii) As the equivalent stiffness increases, the instability modes in Figure 8b–e are essentially the same: the end of the latticed shell tilts integrally to one side, with one side sagging and the other side rising. The instability modes in Figure 8f–h tilt integrally in the opposite direction, with the overall deformation pattern being generally consistent with the previous category.

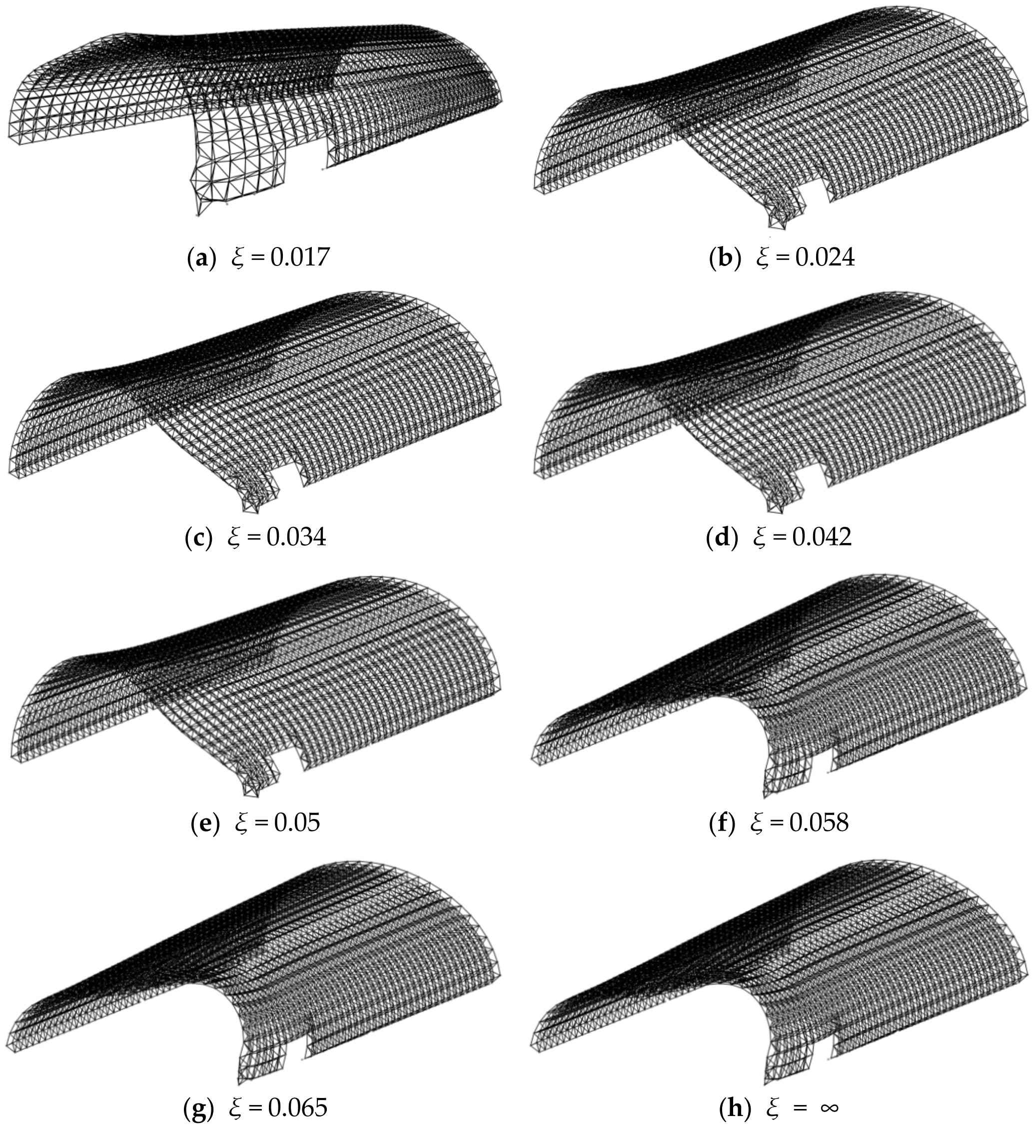

Figure 8. Buckling modes under different equivalent stiffness coefficients.

6. Conclusions

To explore the influence of different equivalent stiffness values on the stability capacity of concrete-pier-supported elliptical cylindrical double-layer reticulated shell structures, this paper establishes a three-dimensional model of the upper elliptical cylindrical double-layer reticulated shell spatial structure. Based on the lower large-section concrete pier support structure, an approximate equivalent stiffness is derived to reasonably set different stiffness levels, and eigenvalue buckling analysis is used to evaluate the stability of the reticulated shell. Under the edge-region loading mode of this example, the following conclusions are obtained:

(1) For reticulated shell structures supported by large-section concrete piers, if a reasonable estimation of the equivalent stiffness is required to provide parameter values of comparable order of magnitude for scientific research, the calculation may be approximately performed using a series cantilever system, assuming that the concrete pier can effectively

restrain the bottom of the steel bearing from rotational deformation. However, it should be noted that this method cannot be used to obtain the exact value of the equivalent stiffness.

(2) Increasing the equivalent support stiffness can enhance the stability capacity of the structure to a certain extent. However, this benefit is more sensitive in the low-stiffness range. As the stiffness increases, the sensitivity gradually decreases, indicating that there is a threshold for the contribution of equivalent stiffness to the load-carrying capacity. In practice, when the applied equivalent stiffness is relatively large, it is recommended to avoid continuing to adopt measures of increasing the equivalent stiffness to improve the stability capacity as much as possible.

(3) Simply applying rigid link constraints laterally at the support joints (assuming infinite equivalent stiffness) will overestimate the stability capacity of the structure to a certain extent.

(4) Under the edge local load mode, when the equivalent stiffness at the supports is relatively low, the instability mode of the reticulated shell appears as a local uplift at the end; as the stiffness gradually increases, its instability mode changes to overall lateral tilting instability.

(5) This paper uses eigenvalue buckling analysis to evaluate the stability of the elliptical cylindrical double-layer reticulated shell structure. This method can usually only obtain a relatively rough stability capacity. The actual stability capacity of the structure needs to be predicted using nonlinear buckling analysis techniques, usually considering factors such as geometric imperfections and geometric nonlinearity. These works will continue to be followed up in future research.

Author Contributions: Conceptualization, P.M.; Methodology, P.M.; Software, P.M.; Investigation, P.M. and S.J.; Writing—original draft, P.M. and S.J.; Writing—review & editing, S.J.; Supervision, S.J.; Funding acquisition, P.M. and S.J. All authors have read and agreed to the published version of the manuscript.

Funding: This research was funded by the 2025 'Enlighten' Talent Training Program Project (grant No. 2025QZ-04), 2026 Gansu Province University Young Doctoral 'Enterprise & Park Entry' Program (grant No. 2026QB-103) and the Integrated Material-Performance-Structure Technology for Performance Enhancement of Composite Materials and Its Engineering Application Demonstration (grant No. 2026CYZC-068).

Data Availability Statement: The original contributions presented in this study are included in the article. Further inquiries can be directed to the corresponding authors.

Conflicts of Interest: The authors declare no conflicts of interest.

References

1. Chilton, J. *Space Grid Structures*; Butterworth-Heinemann: Oxford, UK, 2000.
2. Liu, F.; Xu, T.; Chan, Y.W.S.; Tsavdaridis, K.D. Grid Optimization of Free-Form Spatial Structures Considering the Mechanical Properties. *Buildings* **2024**, *14*, 3191. [CrossRef]
3. Xue, S.D. Recent Development and Engineering Practice of Spatial Structure s in China. *Steel Constr. (Chin. Engl.)* **2020**, *35*, 1–16. [CrossRef]
4. Chen, Z.; Lin, H.; Li, X.; Liu, H.; Li, Z. Equivalent Model Simplification Method for Failure State Study of Large-Span Space Grid Arch Structure. *Structures* **2025**, *75*, 108671. [CrossRef]
5. Fischer, A.W.; Guest, J.K.; Schafer, B.W. Topology Optimization of Steel Deck Building Diaphragms. *J. Constr. Steel Res.* **2022**, *191*, 107186. [CrossRef]
6. Zhou, Y.; Zhang, C. Study on the Distribution of Survival Space in Grid Structures Subjected to Overload Collapse. *J. Anhui Univ. Technol. (Nat. Sci.)* **2026**, *43*, 329–338. [CrossRef]
7. Liu, H.; Lv, Y.; Wang, F.; Li, G.; Liu, L.; Pei, B.; Zhou, Z. Dynamic Experimental Study on Anti-Progressive Collapse of Polyline-Shaped Large-Span Double-Layer Grid Space Structure. *Sci. Rep.* **2025**, *15*, 35999. [CrossRef] [PubMed]

8. Shahbazi, Y.; Abdkarimi, M.; Ahmadnejad, F.; Mokhtari Kashavar, M.; Fotouhi, M.; Pedrammehr, S. Comparative Study of Optimal Flat Double-Layer Space Structures with Diverse Geometries through Genetic Algorithm. *Buildings* **2024**, *14*, 2816. [CrossRef]
9. Gioncu, V. Buckling of Reticulated Shells: State-of-the-Art. *Int. J. Space Struct.* **1995**, *10*, 1–46. [CrossRef]
10. Ferretti, M.; D'Annibale, F. Buckling of Planar Micro-Structured Beams. *Appl. Sci.* **2020**, *10*, 6506. [CrossRef]
11. Xiang, P.; Chen, Y.; Shao, Z.; Peng, X.; Liu, Z.; Chen, W.; Wang, Q. Stochastic Analysis of FG-CNTRC Conical Shell Panels Based on a Perturbation Stochastic Meshless Method without Partial Derivative. *Adv. Eng. Softw.* **2025**, *201*, 103832. [CrossRef]
12. Tian, L.; Wei, J.; Huang, Q.; Ju, J.W. Collapse-Resistant Performance of Long-Span Single-Layer Spatial Grid Structures Subjected to Equivalent Sudden Joint Loads. *J. Struct. Eng.* **2021**, *147*, 04020309. [CrossRef]
13. Luo, T.; Zhao, Y.; Chen, Y.; Zhang, X. Image Vision-Based Prediction Method for Buckling Instability of in-Service Space Grid Steel Tube Members. *Structures* **2025**, *79*, 109596. [CrossRef]
14. *JGJ 7-2010*; Technical Specification for Space Frame Structures. China Architecture & Building Press: Beijing, China, 2011.
15. Liu, F.; Jin, D.; Li, X.; Wei, G. Equivalent Continuum Modeling Method for Transient Response Analysis of Large Space Truss Structures with Nonlinear Elastic Joints. *Acta Mech.* **2023**, *234*, 3499–3517. [CrossRef]
16. Wang, Y.; Jiang, J.H. Research on the mechanical behavior effect of concrete support for large-span spatial grid structural models and simplified analysis method. *Build. Struct.* **2019**, *49*, 43–47. [CrossRef]
17. Gao, Y.; Yang, X.J.; Jiao, X.Z. Restraint state analysis of the support of flat space truss. *Coal Eng.* **2022**, *54*, 26–31. [CrossRef]
18. Saleh Tabari, M.H.; Khojastehmehr, F.; Filz, G.H. A-T-G Louvers: A Novel Geometry and Material Driven Spatial Syntax for Flexible Structures. *Archit. Struct. Constr.* **2025**, *5*, 32. [CrossRef]
19. *GB 50009-2012*; Load Code for the Design of Building Structures. China Architecture & Building Press: Beijing, China, 2013.

https://doi.org/10.3390/buildings16183737